The Astrophysical Journal, 846:54 (11pp), 2017 September 1 https://doi.org/10.3847/1538-4357/aa80df

Dynamical Properties of Internal Shocks Revisited

Asaf Pe'er[1], Killian Long[1], and Piergiorgio Casella[2]
[1] Physics Department, University College Cork, Cork, Ireland
[2] INAF, Osservatorio Astronomico di Roma, Via Frascati 33, I-00078 Monteporzio Catone, Italy
Received 2016 October 26; revised 2017 June 12; accepted 2017 July 16; published 2017 August 31

Abstract

Internal shocks between propagating plasma shells, originally ejected at different times with different velocities, are believed to play a major role in dissipating the kinetic energy, thereby explaining the observed light curves and spectra in a large range of transient objects. Even if initially the colliding plasmas are cold, following the first collision, the plasma shells are substantially heated, implying that in a scenario of multiple collisions, most collisions take place between plasmas of non-zero temperatures. Here, we calculate the dynamical properties of plasmas resulting from a collision between arbitrarily hot plasma shells, moving at arbitrary speeds. We provide simple analytical expressions valid for both ultrarelativistic and Newtonian velocities for both hot and cold plasmas. We derive the minimum criteria required for the formation of the two-shock wave system, and show that in the relativistic limit, the minimum Lorentz factor is proportional to the square root of the ratio of the initial plasmas enthalpies. We provide basic scaling laws of synchrotron emission from both the forward and reverse-shock waves, and show how these can be used to deduce the properties of the colliding shells. Finally, we discuss the implications of these results in the study of several astronomical transients, such as X-ray binaries, radio-loud quasars, and gamma-ray bursts.

Key words: gamma-ray burst: general – hydrodynamics – plasmas – shock waves – stars: jets – X-rays: binaries

1. Introduction

Light curves of many astronomical transients that are characterized by strong outflows (jets) show substantial variability, observed on timescales as fast as milliseconds and possibly even faster. Several examples include blazars (Marscher 1980), gamma-ray bursts (GRBs; Norris et al. 1996), and X-ray binaries (XRBs; Fender 2001). A leading model proposed to explain these variable light curves is the internal-shocks model. The basic idea is that variability within the inner engine results in fluctuations in the ejection of plasmas. Thus, the ejected material propagates as a collection of "plasma shells." Each individual shell is accelerated and then propagates at some terminal velocity that is independent of the terminal velocities of the other plasma shells. At a second stage, shells that were ejected at later times but with faster speeds catch up with the slower shells ahead. The collision between the plasma shells results in the formation of two shock waves (forward and reverse) that propagate into the slow and fast shells, respectively. These shock waves dissipate part of the kinetic energy of the shells, which is then radiated away. Following the collision, the colliding shells are assumed to merge and continue propagating together (i.e., the collision is considered as a plastic collision), and they are therefore subject to a subsequent collision with a third incoming, faster shell. This scenario of multiple collisions therefore results in the observed variable light curve.

Such models were proposed to explain the knots in active galactic nucleus (AGN) jets (Rees 1978). They have been in wide use since the 1990s to explain the rapid variability observed during the prompt phase of many GRBs (e.g., Rees & Meszaros 1994; Fenimore et al. 1996; Kobayashi et al. 1997; Sari & Piran 1997; Daigne & Mochkovitch 1998; Panaitescu et al. 1999; Ramirez-Ruiz & Fenimore 2000; Guetta et al. 2001; Mészáros et al. 2002; Nakar & Piran 2002; Kino et al. 2004; Cantó et al. 2013), as well as in blazars (Sikora et al. 1994; Ghisellini 1999; Spada et al. 2001; Böttcher & Dermer 2010; Mimica & Aloy 2010). In recent years, similar models were applied in the study of variable emission from XRBs (Kaiser et al. 2000; Miller-Jones et al. 2005; Jamil et al. 2010; Malzac 2013, 2014; Drappeau et al. 2015) as well as tidal disruption events (Wang & Cheng 2012). See Pe'er (2014) for a review on the similarities between these objects. Indeed, the hydrodynamical properties of the shock waves as well as the colliding shells have long been investigated in the nonrelativistic as well as in the relativistic regimes (Blandford & McKee 1976; Sari & Piran 1995).

Despite its considerable popularity, it should be stressed that it is still unclear today whether internal shocks by themselves are the leading mechanism that produces the observed signal in these objects. In the context of GRBs, for example, there are two main drawbacks of this model. First, the relatively low efficiency in energy conversion, as only the differential kinetic energy can be dissipated. Several authors found that the typical efficiency of energy conversion that can be expected in a multiple-shell collision is only a few to a few tens of percent (Kobayashi et al. 1997; Daigne & Mochkovitch 1998; Kumar 2000; Guetta et al. 2001; Freedman & Waxman 2001; Ioka et al. 2006). This result, however, depends on the velocity distribution of the ejected shells, and can become substantially higher under the appropriate conditions (Beloborodov 2000; Kobayashi & Sari 2001). The second drawback (in the context of GRBs) is accumulating evidence in recent years that a thermal component may play an important role in explaining at least part of the observed spectra in a significant minority of GRBs (Ryde 2004, 2005; Pe'er 2008; Lazzati et al. 2009; Ryde & Pe'er 2009; Guiriec et al. 2011; Ryde et al. 2011; Axelsson et al. 2012). As this component originates from the photosphere, a dominant thermal component implies that a substantial energy dissipation at larger radii may be unnecessary. Nonetheless, in most cases in which a thermal component is observed, it is accompanied

by an addition nonthermal part (e.g., Pe'er 2015, and references therein).

While the validity of the internal-shocks model as a leading energy dissipation mechanism is uncertain, the main alternative dissipation models, namely magnetic reconnection (Coroniti 1990; Usov 1992; Thompson 1994; Lyubarsky & Kirk 2001; Drenkhahn 2002; Drenkhahn & Spruit 2002), suffers an even higher degree of uncertainty. For example, as the rate of reconnection depends on the magnetohydrodynamic (MHD) turbulence, it is difficult to be assessed from first principles without detailed specification of the environment. It is therefore no surprise that no consensus on the origin of dissipation has been achieved to date. An in-depth discussion of the current observational status in GRBs and its implications appears in several recent reviews (e.g., Piran 2004; Fox & Mészáros 2006; Mészáros 2006; Woosley & Bloom 2006; Zhang 2007; Gehrels et al. 2009; Meszaros & Rees 2014; Zhang 2014; Kumar & Zhang 2015, and references therein).

Given these uncertainties, a more in-depth study is needed on the underlying physics of the different models. Indeed, within the framework of the internal-shocks model, one thing in common to nearly all studies carried out so far is that a detailed description of the shocked-plasma conditions was made based on the assumption that the colliding plasmas are initially cold (Sari & Piran 1995). While the expanding plasma shells lose their energy adiabatically during the expansion, the shock waves formed in each collision substantially heat the plasma. Thus, even if initially the plasmas are cold, in a scenario of multiple collisions, the colliding plasmas are in general not expected to be cold. While this fact was considered by several authors in calculating the overall efficiency of energy conversion (Panaitescu et al. 1999; Beloborodov 2000; Kumar & Piran 2000; Guetta et al. 2001; Spada et al. 2001; Kino et al. 2004; Jamil et al. 2010; Malzac 2014), no detailed description of the shocked-plasma properties has been calculated so far in the general scenario of arbitrary hot plasmas colliding at arbitrary velocities.

This calculation is of particular importance for two reasons. First, when arbitrary hot plasmas collide, the conditions for the formation of the system with two shock waves are not always fulfilled. As a result, the amount of energy dissipated in such a collision can be substantially smaller than if shock waves are formed. Second, even if shock waves are formed, the expected spectra depend on the energy density and energy per particle in the shocked region, which are in general different than in the cold-plasma collision scenario (Zhang & Mészáros 2002). Thus, in order to provide accurate calculations of the expected light curve and spectra, the conditions at the shocked plasma need to be determined.

A scenario of a cold shell interacting relativistically with a hot ($e \gg nm_pc^2$, where e and n are the energy and number densities, m_p is the proton mass, and c is the speed of light) expanding shell that was slowed down by interacting with the ambient medium was considered by Kumar & Piran (2000). A relative Lorentz factor between the colliding shells of 1.25 was found to represent the scenario considered in that work well. The results indeed indicate that the plasma properties following the collision deviate from the plasma properties expected in the cold-cold shell collisions.

In this work, we calculate the properties of the shocked plasma following the collision of two arbitrarily hot plasma shells. We consider a simple 1D model that enables us to provide simple analytic estimations of the thermodynamic properties of the shocked plasmas in the various regimes. As we show below, one needs to discriminate not only between the relativistic and nonrelativistic scenarios, but the analytical solutions also depend on the energy densities of the plasmas. We thus discriminate between "cold," "cool", and "hot" plasmas (see definitions in Section 2 below). We derive the minimum criteria for the formation of such shocks in the different scenarios, as well as the properties (velocity, energy density, and energy per particle) of the shocked plasma. In Section 3 we provide a full numerical solution, which can be used for arbitrary plasma properties and further serves to validate and demonstrate the analytical approximations in the different regimes. In Section 4 we discuss observational consequences of the model, and in particular, we show that the efficiency in energy conversion is different than previous claims because of the need to include a pressure term. We further demonstrate how the properties of the synchrotron emission can be used to probe the properties of the colliding shells, before summarizing in Section 5.

2. Basic Setup

We consider a slab of (non-magnetized) plasma shell ("slow shell") that propagates at some arbitrary speed $\beta_1 = v_1/c$ (corresponding Lorentz factor Γ_1) in the laboratory frame. A second plasma shell ("fast shell") that propagates at velocity $\beta_4 > \beta_1$ collides with the slow shell. At sufficiently high β_4, two shock waves are formed as a result of the collision: a forward shock propagating into the slow shell, and a reverse shock propagating into the fast shell. A contact discontinuity separates the shocked slow-shell material from the shocked fast-shell material.

Following the collision, there are four different regimes: (1) the slow shell, (2) the shocked slow shell, (3) the shocked fast shell, and (4) the fast-shell material. The velocities of the four regimes are β_i, $(i = 1..4)$ and the corresponding Lorentz factors are $\Gamma_i = (1 - \beta_i)^{-1/2}$. The thermodynamical quantities n_i, e_i, p_i, and $\omega_i = e_i + p_i$ (number density, internal energy density, pressure, and enthalpy, respectively) are measured in each of the fluid (shells) rest-frames. We further denote the speed of the forward and reverse-shock waves in the laboratory frame by β_{fs}, β_{rs}, respectively (corresponding to the Lorentz factors Γ_{fs}, Γ_{rs}).

The system considered therefore contains a total of 18 free parameters (β_i, n_i, e_i, p_i $[i = 1..4]$, β_{fs}, β_{rs}). The shock jump conditions, namely conservation of particle, energy, and momentum flux densities at each shock wave, provide 6 equations. Two more equations are provided by equating the pressures and velocities along the contact discontinuity. An additional 4 equations of state, of the form $p_i = (\hat{\gamma}_i - 1)(e_i - n_i)$, where $\hat{\gamma}_i$ is the adiabatic index in region i, complete a total of 12 equations connecting the velocities and thermodynamic quantities in all four regimes. Thus, by specifying a total of six boundary conditions, namely the initial velocities, and the number and energy densities in the slow- and fast-plasma shells (β_1, β_4, n_1, n_4, e_1, e_4), the velocities and thermodynamic properties of all four regions of the system are fully determined.[3]

[3] We assume that the conditions are homogeneous within each regime. This approximation is reasonable as long as the initial colliding shells are not too wide. This can easily be justified in the shocked regions, which are subsonic.

In this and the following sections we provide a complete solution in the planar case. Clearly, in the most general scenario, the values of all 18 parameters can only be determined numerically. However, as we show here, simple analytical solutions exist in the limiting cases of relativistic ($\Gamma_4 \gg \Gamma_1$) as well as Newtonian ($\beta_4, \beta_1 \ll 1$) plasma shell velocities. In this section we first derive the analytical solutions before providing a few examples of the full numerical solution in Section 3 below.

2.1. Analytical Solution: Basic Equations

For simplicity, we assume in the calculations below that the slow plasma is at rest ($\beta_1 = 0,\ \Gamma_1 = 1$). This can be viewed as a specific case, but also as conducting the calculations in the rest-frame of the slow-plasma shell. Toward the end of the next section, we transform the derived results into the laboratory frame, in which $\Gamma_1 \geqslant 1$ is arbitrary. Thus, in the calculations below, Γ_2 is the Lorentz factor of the shocked slow plasma (region (2)) in the rest-frame of region (1), etc.

The forward-shock jump conditions follow from the continuity of energy ($T^{01} = \omega\Gamma^2\beta$), momentum ($T^{11} = \omega\Gamma^2\beta^2 + p$), and particle ($n\Gamma\beta$) flux densities in the shock frame. Here, $T^{\mu\nu} = \omega u^\mu u^\nu + p\eta^{\mu\nu}$ is the stress- energy tensor, u^μ is the four-velocity, and $\eta^{\mu\nu}$ is the metric tensor. In their most general form, the forward-shock jump conditions can be written in the form (Blandford & McKee 1976; Wiersma 2007)

$$\frac{e_2}{n_2} = \Gamma_2\frac{\omega_1}{n_1} - \frac{p_1}{n_2}, \tag{1}$$

$$p_2 - p_1 = \frac{(\Gamma_2\beta_2)^2 n_2\omega_1}{n_2 - \Gamma_2 n_1}. \tag{2}$$

Similarly, the reverse-shock jump conditions are written as

$$\frac{e_3}{n_3} = \bar{\Gamma}_3\frac{\omega_4}{n_4} - \frac{p_4}{n_3}, \tag{3}$$

$$p_3 - p_4 = \frac{(\bar{\Gamma}_3\bar{\beta}_3)^2 n_3\omega_4}{n_3 - \bar{\Gamma}_3 n_4}. \tag{4}$$

Here, $\bar{\Gamma}_3 = \Gamma_3\Gamma_4(1 - \beta_3\beta_4)$ is the Lorentz factor of the shocked material in region (3) relative to the unshocked fast shell in region (4), and $\bar{\beta}_3 = (1 - \bar{\Gamma}_3^{-2})^{1/2}$ is the corresponding velocity.

2.2. Relativistic Collision

In the ultrarelativistic case, we consider the scenario where $\Gamma_4 \gg \Gamma_2 = \Gamma_3 \gg 1$. Under this assumption,

$$\bar{\Gamma}_3 \simeq \frac{1}{2}\left(\frac{\Gamma_4}{\Gamma_3} + \frac{\Gamma_3}{\Gamma_4}\right) \approx \frac{\Gamma_4}{2\Gamma_2}. \tag{5}$$

Since it is always true that $n_2 \geqslant n_1$ and $n_3 \geqslant n_4$ (and clearly $\omega_1 \geqslant p_1,\ \omega_4 \geqslant p_4$), it is safe to neglect the second terms in the right-hand sides of Equations (1) and (3). Using the equations of state for regions (2) and (3), with the help of the modified Equations (1) and (3), the pressures in regions (2) and (3) can be written as

$$\begin{aligned} p_2 &= (\hat{\gamma}_2 - 1)n_2\left(\tfrac{e_2}{n_2} - 1\right) \\ &\simeq (\hat{\gamma}_2 - 1)n_2\Gamma_2\tfrac{\omega_1}{n_1}; \\ p_3 &\simeq (\hat{\gamma}_3 - 1)\omega_4\bar{\Gamma}_3\tfrac{n_3}{n_4}. \end{aligned} \tag{6}$$

Using these results in Equations (2), (4), and neglecting $p_1 \ll p_2$ as well as $p_4 \ll p_3$ (which is correct in the ultrarelativistic limit), one obtains

$$\frac{n_2}{n_1} = \frac{\hat{\gamma}_2}{\hat{\gamma}_2 - 1}\Gamma_2; \quad \frac{n_3}{n_4} = \frac{\hat{\gamma}_3}{\hat{\gamma}_3 - 1}\bar{\Gamma}_3. \tag{7}$$

In order to proceed, we use the fact that in the relativistic limit, the adiabatic indices are $\hat{\gamma}_2 = \hat{\gamma}_3 = 4/3$. Using these results, as well as the approximation derived in Equation (5) in Equation (6), the requirement $p_2 = p_3$ leads to

$$\begin{aligned} \Gamma_2 = \Gamma_3 &\simeq \sqrt{\frac{\Gamma_4}{2}}\left(\frac{\omega_4}{\omega_1}\right)^{1/4}, \\ \bar{\Gamma}_3 &\simeq \sqrt{\frac{\Gamma_4}{2}}\left(\frac{\omega_1}{\omega_4}\right)^{1/4}. \end{aligned} \tag{8}$$

Using Equations (1), (3) and (7), the energy per particle and the energy densities in regions (2) and (3) are given by

$$\begin{aligned} &\frac{e_2}{n_2} \simeq \sqrt{\tfrac{\Gamma_4}{2}}\tfrac{\omega_1^{3/4}\omega_4^{1/4}}{n_1}; \quad \frac{e_3}{n_3} \simeq \sqrt{\tfrac{\Gamma_4}{2}}\tfrac{\omega_1^{1/4}\omega_4^{3/4}}{n_4}; \\ &e_2 = e_3 \simeq \tfrac{\hat{\gamma}_2}{\hat{\gamma}_2 - 1}\tfrac{\Gamma_4}{2}\omega_1^{1/2}\omega_4^{1/2} = 2\Gamma_4\omega_1^{1/2}\omega_4^{1/2}, \end{aligned} \tag{9}$$

where in the last line, we took $\hat{\gamma}_2 = \hat{\gamma}_3 = 4/3$.

The results derived in Equation (9) can further be used to set a minimum criterion on the Lorentz factor of the fast shell, Γ_4, that enables the existence of the two-shock system if the colliding plasma shells are initially hot. Writing $e_i = \omega_i/\hat{\gamma}_i + (\hat{\gamma}_i - 1)n_i/\hat{\gamma}_i \approx \omega_i/\hat{\gamma}_i$, the requirements $e_2 \geqslant e_1$ and $e_3 > e_4$ are translated into the criteria

$$\begin{aligned} \Gamma_4 &\geqslant 2\frac{\hat{\gamma}_2 - 1}{\hat{\gamma}_1\hat{\gamma}_2}\sqrt{\frac{\omega_1}{\omega_4}} = \frac{3}{8}\sqrt{\frac{\omega_1}{\omega_4}}, \\ \Gamma_4 &\geqslant 2\frac{\hat{\gamma}_3 - 1}{\hat{\gamma}_4\hat{\gamma}_3}\sqrt{\frac{\omega_4}{\omega_1}} = \frac{3}{8}\sqrt{\frac{\omega_4}{\omega_1}}, \\ \rightarrow \Gamma_4 &\geqslant \frac{3}{8}\max\left\{\sqrt{\frac{\omega_4}{\omega_1}}, \sqrt{\frac{\omega_1}{\omega_4}}\right\}, \end{aligned} \tag{10}$$

where we took $\hat{\gamma}_i = 4/3$ in all four regimes, which is valid for hot plasmas. This minimum value of the Lorentz factor can be understood as follows: as the Lorentz factor of the fast shell (Γ_4) decreases, either the forward or reverse shock eventually ceases to be relativistic, and the amount of energy dissipated from the (initially hot) plasma shells decreases. When this criterion is met, (at least) one of the two shock waves ceases to exist. Instead, a rarefaction wave will be created and propagate into the hot plasma, while the second shock wave could still exist.

We emphasize that the result of Equation (10) sets the minimum criteria on the Lorentz factor, originating from the physical requirement that the shock waves are capable of dissipating the kinetic energy of the shell. To these criteria, one must add the underlying assumption taken in this section that

$\Gamma_4 \gg \Gamma_2 \gg 1$. These criteria are further validated numerically (see Section 3 below).

Finally, we note that a Lorentz transformation to the *laboratory frame*, in which $\Gamma_1^L \equiv \Gamma_1 \gg 1$, yields $\Gamma_2^L = \Gamma_1\Gamma_2(1+\beta_1\beta_2) \simeq 2\Gamma_1\Gamma_2$, and similarly $\Gamma_4^L \simeq 2\Gamma_1\Gamma_4$. The Lorentz factor of the shocked plasmas is therefore given by (Equation (8)),

$$\Gamma_2^L = \sqrt{\Gamma_1^L\Gamma_4^L}\left(\frac{\omega_4}{\omega_1}\right)^{1/4}. \tag{11}$$

2.3. Newtonian Collision

We next consider the Newtonian (nonrelativistic) case, in which the relative motion between the two colliding shells is nonrelativistic or transrelativistic at most. We do allow the colliding plasmas to be arbitrarily hot, however. Similar to the relativistic treatment, we initially assume $\Gamma_1 = 1$.

In this case, it is handy to define the internal energy (excluding the rest mass) ϵ_1 by $\epsilon_1 \equiv e_1 - n_1$. When writing the energy density in region (1) as $e_1 = n_1 + \epsilon_1$, the forward-shock jump conditions (Equations (1) and (2)) can be written as a quadratic equation in the ratio of the proper densities at both sides of the forward-shock wave,

$$\begin{aligned}&\left(\frac{n_2}{n_1}\right)^2\left[\Gamma_2\left(1+\hat{\gamma}_1\frac{\epsilon_1}{n_1}\right)-1\right]-\left(\frac{n_2}{n_1}\right)\\&\times\left[\left(1+\hat{\gamma}_1\frac{\epsilon_1}{n_1}\right)\left(2+\frac{\hat{\gamma}_2}{\hat{\gamma}_2-1}\Gamma_2^2\beta_2^2\right)-(\Gamma_2+1)\right]\\&+\hat{\gamma}_1\Gamma_2\frac{\epsilon_1}{n_1}=0\end{aligned} \tag{12}$$

(with a similar equation holding for the reverse shock). Note that Equation (12) is exact for all velocities. In order to obtain a useful approximation in the Newtonian regime, one needs to (i) approximate $\Gamma_2 \simeq 1+\beta_2^2/2$; and (ii) discriminate between different regimes, based on the value of ϵ_1: hot, cool, and cold.

In the hot regime, $\epsilon_1/n_1 \gg 1$. The ratio of densities at both sides of the shock waves becomes

$$\begin{aligned}\left(\frac{n_2}{n_1}\right)_{\rm hot} &\simeq 1+\frac{\beta_2}{\sqrt{\hat{\gamma}_2-1}}+\frac{\beta_2^2}{2(\hat{\gamma}_2-1)}\\&=1+\sqrt{3}\,\beta_2+\frac{3}{2}\beta_2^2,\end{aligned} \tag{13}$$

where we took $\hat{\gamma}_1 = \hat{\gamma}_2 \simeq 4/3$ in the last equality. When we use this result in Equation (1), the energy density in region (2) is given by

$$\begin{aligned}e_2 &\simeq \epsilon_1\left(1+\frac{\hat{\gamma}_1}{\sqrt{\hat{\gamma}_2-1}}\beta_2+\frac{\hat{\gamma}_1\hat{\gamma}_2}{2(\hat{\gamma}_2-1)}\beta_2^2\right)\\&=\epsilon_1\left(1+\frac{4}{\sqrt{3}}\beta_2+\frac{8}{3}\beta_2^2\right).\end{aligned} \tag{14}$$

Clearly, a similar equation holds for the energy density in region (3).

In the opposite limit, that is, in the cool/cold limit, namely $\epsilon_1/n_1 \ll 1$, we proceed as follows. First, in the nonrelativistic limit, $\beta_2 \ll 1$, the ratio of densities derived from the shock jump conditions (Equation (12)) can be put in the form

$$\begin{aligned}&\left(\frac{n_2}{n_1}\right)^2\left[\frac{\beta_2^2}{2}+\hat{\gamma}_1\frac{\epsilon_1}{n_1}\left(1+\frac{\beta_2^2}{2}\right)\right]-\left(\frac{n_2}{n_1}\right)\\&\times\left[\left(\frac{\hat{\gamma}_2+1}{\hat{\gamma}_2-1}\right)\frac{\beta_2^2}{2}+2\hat{\gamma}_1\frac{\epsilon_1}{n_1}\left(1+\frac{\hat{\gamma}_2}{\hat{\gamma}_2-1}\frac{\beta_2^2}{2}\right)\right]\\&+\hat{\gamma}_1\frac{\epsilon_1}{n_1}\left(1+\frac{\beta_2^2}{2}\right)=0.\end{aligned} \tag{15}$$

We next discriminate between the cool case, in which $\epsilon_1/n_1 \gg \beta_2^2$, and the opposite case, the cold case, in which $\epsilon_1/n_1 \ll \beta_2^2$. In the cool scenario, the ratio of densities and the energy density in region (2) are given by

$$\begin{aligned}&\left(\frac{n_2}{n_1}\right)_{\rm cool} \simeq 1+\frac{1}{\sqrt{\hat{\gamma}_1(\hat{\gamma}_2-1)\frac{\epsilon_1}{n_1}}}\beta_2+\frac{3-\hat{\gamma}_2}{4\hat{\gamma}_1(\hat{\gamma}_2-1)\frac{\epsilon_1}{n_1}}\beta_2^2,\\&(e_2)_{\rm cool} \simeq n_1\left[1+\frac{\epsilon_1}{n_1}+\frac{1}{\sqrt{\hat{\gamma}_2-1}}\left(\sqrt{\hat{\gamma}_1\frac{\epsilon_1}{n_1}}+\frac{1}{\sqrt{\hat{\gamma}_1\frac{\epsilon_1}{n_1}}}\right)\beta_2\right].\end{aligned} \tag{16}$$

In this case, the value of the adiabatic index is not known a priori (see discussion in Section 3 below).

In the cold scenario, $\epsilon_1/n_1 \ll \beta_2^2$, a similar calculation yields

$$\begin{aligned}\left(\frac{n_2}{n_1}\right)_{\rm cold} &\simeq \left(\frac{\hat{\gamma}_2+1}{\hat{\gamma}_2-1}\right)+\frac{2\hat{\gamma}_1}{\hat{\gamma}_2+1}\frac{\epsilon_1}{n_1}-\frac{8\hat{\gamma}_1}{(\hat{\gamma}_2+1)(\hat{\gamma}_2-1)}\frac{\epsilon_1}{n_1\beta_2^2}\\&=4+\left(\frac{5}{4}-\frac{15}{2\beta_2^2}\right)\left(\frac{\epsilon_1}{n_1}\right),\\(e_2)_{\rm cold} &\simeq n_1\left[\left(\frac{\hat{\gamma}_2+1}{\hat{\gamma}_2-1}\right)\left(1+\frac{\beta_2^2}{2}\right)-\frac{8\hat{\gamma}_1}{(\hat{\gamma}_2+1)(\hat{\gamma}_2-1)}\right.\\&\left.\times\left(\frac{\epsilon_1}{n_1\beta_2^2}\right)+\frac{3\hat{\gamma}_1+1}{\hat{\gamma}_2+1}\left(\frac{\epsilon_1}{n_1}\right)\right]\\&=n_1\left[4\left(1+\frac{\beta_2^2}{2}\right)+\left(\frac{9}{4}-\frac{15}{2\beta_2^2}\right)\left(\frac{\epsilon_1}{n_1}\right)\right],\end{aligned} \tag{17}$$

where we used $\hat{\gamma}_1 = \hat{\gamma}_2 = 5/3$ in the last equality. We further point out that given an arbitrary value of $0 < (\epsilon_1/n_1) < 1$, for very low relative velocities between the plasma shells, the plasma can be considered as "cool," while at higher velocities it can be regarded as "cold."

The results presented in Equations (12)–(17) are of course symmetric with respect to the reverse shock, and are obtained by replacing quantities in regions (1), (2) with those in regions (4), (3), respectively, and exchanging β_2 with $\bar{\beta}_3 \simeq \beta_4 - \beta_2$. Using these replacements, one can use the requirement $p_2 = p_3$ to determine the shocked-plasma velocity, $\beta_2 = \beta_3$ as a function of the colliding plasmas parameters (n_1, e_1, n_4 and e_4) as well as their relative velocities β_4 in the different regimes. The results of the various scenarios are summarized in Table 1.

The results in Table 1 can also be used to place constraints on the minimum relative velocities between the shells (β_4) that enable the formation of the double-shock structure. These limits originate from the requirements (a) $\beta_2 \geqslant 0$ and (b) $\bar{\beta}_3 = \beta_4 - \beta_2 \geqslant 0$. In the first scenario considered in Table 1, that of interaction between two cold plasmas, β_2 is always smaller than β_4 and therefore there is no restriction: a double-shock structure will always form for each value of $\beta_4 > 0$. However, this is an exceptional case: in all other scenarios, in

Table 1
Shocked-plasma Velocities in the Various Cases

Scenario	Shocked-shell Velocities, $\beta_2 = \beta_3$
(a) cold → cold	$\beta_4 \frac{\sqrt{\frac{n_4}{n_1}}}{\sqrt{\frac{n_4}{n_1}}+1}$
(b) cold → cool	$\beta_4 - \left[\frac{1}{2}\left(\frac{\hat{\gamma}_2-1}{\hat{\gamma}_3-1}\right)\left(\frac{n_1}{n_4}\right)\left(\frac{\epsilon_1}{n_1}\right)\right]^{1/2}$
(c) cold → hot	same as (b), cold → cool
(d) cool → cool	$\frac{(\hat{\gamma}_3-1)\epsilon_4-(\hat{\gamma}_2-1)\epsilon_1+(\hat{\gamma}_3-1)\sqrt{\frac{\hat{\gamma}_4}{\hat{\gamma}_4-1}}\sqrt{n_4\epsilon_4}\beta_4}{(\hat{\gamma}_2-1)\sqrt{\frac{\hat{\gamma}_1}{\hat{\gamma}_1-1}}\sqrt{m_1\epsilon_1}+(\hat{\gamma}_3-1)\sqrt{\frac{\hat{\gamma}_4}{\hat{\gamma}_4-1}}\sqrt{n_4\epsilon_4}}$
(e) cool → hot	$\frac{(\hat{\gamma}_3-1)\epsilon_4-(\hat{\gamma}_2-1)\epsilon_1+(\hat{\gamma}_3-1)\sqrt{\frac{\hat{\gamma}_4}{\hat{\gamma}_4-1}}\sqrt{n_4\epsilon_4}\beta_4}{(\hat{\gamma}_2-1)\frac{4}{\sqrt{3}\epsilon_1}+(\hat{\gamma}_3-1)\sqrt{\frac{\hat{\gamma}_4}{\hat{\gamma}_4-1}}\sqrt{n_4\epsilon_4}}$
(f) hot → hot	$\frac{\epsilon_4-\epsilon_1+\frac{4}{\sqrt{3}}\epsilon_4\beta_4}{\frac{4}{\sqrt{3}}(\epsilon_1+\epsilon_4)}$

which at least one of the shells is not completely cold, such a restriction does exist. If β_4 is smaller, then the minimum value set by n_1, n_4, ϵ_1, and ϵ_4, the ram pressure cannot compensate for the excess energy gained by thermalization at the shock front. In these cases, two shocks cannot form. Instead, similar to the relativistic case, a rarefaction wave will form, which will gradually modify the properties of one of the shells.

3. Numerical Solution

In order to validate the analytical approximations presented in Section 2 above as well as to investigate the intermediate velocity (transrelativistic) regime, we wrote a numerical code that solves the dynamical conditions at each of the four regimes—unshocked and shocked-plasma shells that follow the collision of two plasma shells. The code simultaneously solves the set of 12 coupled equations: 3 shock jump conditions each for the forward-shock and reverse-shock waves, equating the pressure and velocity along the contact discontinuity, and 4 equations of state. The results are obtained for a given set of 6 initial conditions: velocity, number and energy densities in regions (1) and (4), the unshocked plasmas.

3.1. Determination of the Adiabatic Indices in the Different Regimes

In order to account for the energy dependence of the adiabatic indices $\hat{\gamma}_i$ in each of the four regimes, we use the prescription derived by Service (1986), which is accurate to 10^{-5}. Since the classical gas law, $p_i = n_i T_i$, holds exactly in all regimes, one can write

$$\frac{e_i}{n_i} = T_i\left(\frac{e_i + p_i}{p_i} - 1\right). \tag{18}$$

We use the approximation derived by Service (1986),

$$\frac{p_i}{e_i + p_i} = 0.36y + 0.036346y^2 - 0.088763y^3 - 0.047698y^4 - 0.083547y^5 + 0.073662y^6, \tag{19}$$

where

$$y \equiv \frac{T_i}{0.36 + T_i}. \tag{20}$$

The results of Equation (19) are tabulated. Thus, for a given ratio e_i/n_i, we use the tabulated results in Equation (18) to infer the temperature T_i in region i.

Once the temperature is known, the adiabatic index in each regime is calculated in a second step using

$$\hat{\gamma}_i = \frac{1}{3}(5 - 1.21937z + 0.18203z^2 - 0.96583z^3 + 2.32513z^4 - 2.39332z^5 + 1.07136z^6), \tag{21}$$

where

$$z \equiv \frac{T_i}{0.24 + T_i}. \tag{22}$$

The dynamical properties of the plasmas in the different regimes are calculated as follows. We first guess a value of the shocked-plasma velocity (more precisely, of $\Gamma_2\beta_2 = \Gamma_3\beta_3$), and solve for the two-shock jump conditions. The value of $\Gamma_2\beta_2$ is then varied until the pressures at each side of the contact discontinuity are equal.

In order to determine the adiabatic index in the shocked regions, the shock jump conditions are solved in iterative way for each value of $\Gamma_2\beta_2$. Following an initial guess of $\hat{\gamma}_2$, $\hat{\gamma}_3$, the shock jump conditions are solved and the values of the specific energies e_2/n_2 and e_3/n_3 are determined. The values of the adiabatic index are then re-calculated, and the calculation is repeated with the new value. We found that convergence is typically very quick, within a few iterations at most.

3.2. Numerical Results

Examples of the numerical results, together with the analytical approximations in the different regimes, are presented in Figures 1–3.

In Figure 1 we calculate the dynamical and thermal properties in all four regimes following the collision of two cold-plasma shells. The first (slow) shell is characterized by a density $n = 1\ \mathrm{cm}^{-3}$ and zero internal energy ($e_1 = n_1 m_e c^2$). The fast-plasma shell is characterized by a higher density of $n_4 = 100\ \mathrm{cm}^{-3}$ and is similarly cold, $e_4 = n_4 m_e c^2$. The density contrast is chosen to be 100 for presentation purposes. We further chose the slow plasma to be motionless, $\beta_1 = 0$. The results are presented as a function of $\Gamma_4\beta_4$, where β_4 is the relative velocity between the shells.

For cold plasmas as considered in Figure 1, there is no lower limit on β_4, i.e., the two-shock system always forms for any value of $\beta_4 > 0$. This system of cold plasmas is in fact identical to the system considered previously by Sari & Piran (1995). In Figure 1(a) we show the shocked-plasma velocity, ($\Gamma_2\beta_2$), in the rest-frame of the slow shell as well as the same velocity in the rest-frame of the unshocked, fast plasma in region (4), denoted by ($\bar{\Gamma}_3\bar{\beta}_3$). The asymptotic approximations in the relativistic (Equations (8)) and nonrelativistic (Table 1(a)) regimes are given by the dashed and dash–dotted lines. To produce the nonrelativistic approximation of the velocities, we replace β_4 with $\Gamma_4\beta_4$. The results show excellent agreement—better than ∼10% for $\Gamma_4\beta_4 \leqslant 2$.

In Figures 1(b) and (c) we show the energy densities and the energy per particle (e_i/n_i) in the shocked-plasma regions (2)

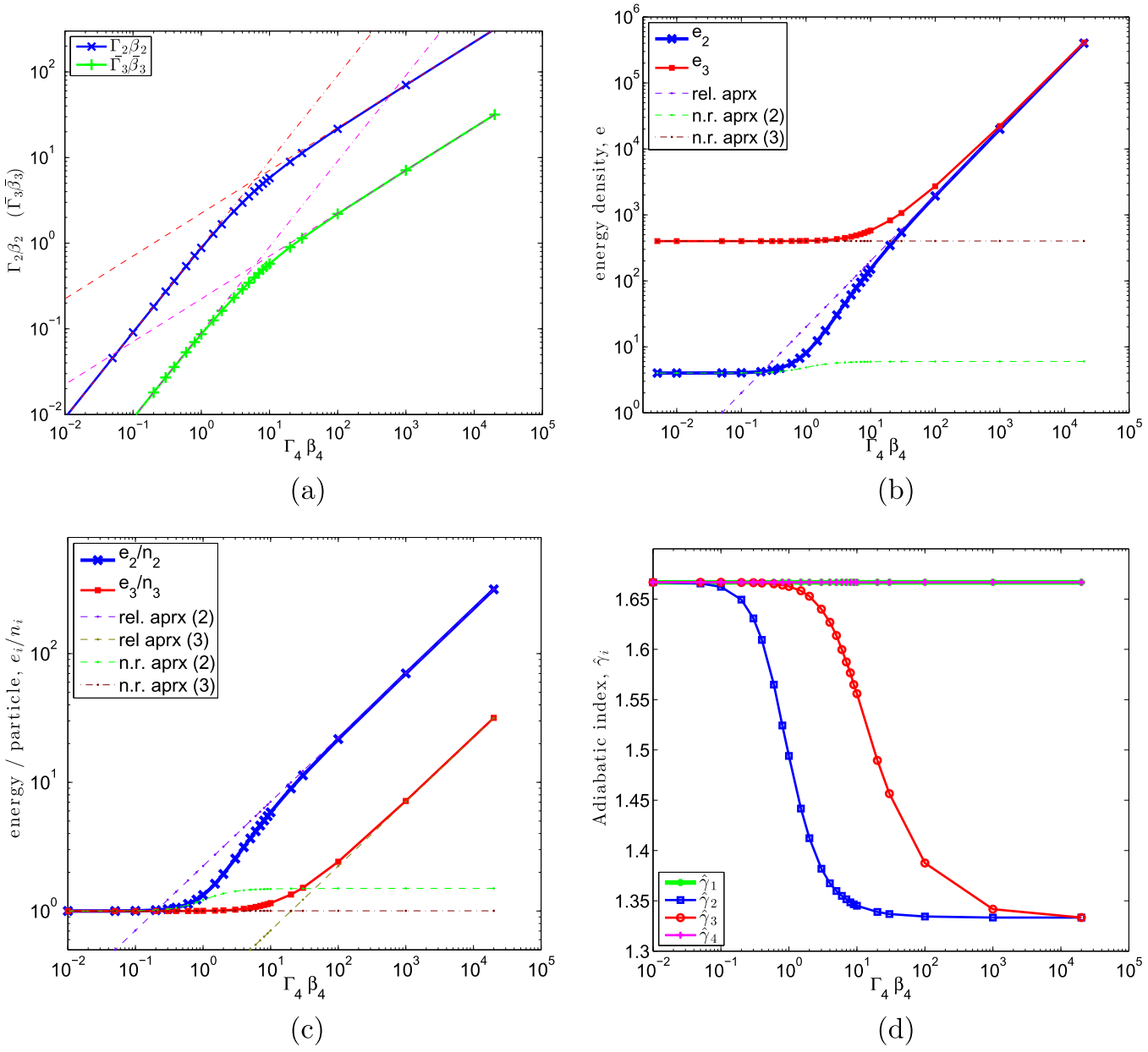

Figure 1. Velocities and thermodynamic properties of the shocked plasma following collision between two cold-plasma shells ($\epsilon_i = 0$, $i = 1, 4$). The parameters considered are $n_1 = 1\ \mathrm{cm}^{-3}$, $\epsilon_1 = 0$, $n_4 = 100\ \mathrm{cm}^{-3}$, $\epsilon_4 = 0$, and $\beta_1 = 0$. Plasma parameters are shown as a function of the fast-shell initial velocity, $\Gamma_4\beta_4$. (a) Velocities of the shocked-plasma regions (2) and (3), as measured in the rest-frame of the slow-plasma shell in region (1) ($\Gamma_2\beta_2$) and the rest-frame of the fast-plasma shell in region (4), ($\bar{\Gamma}_3\bar{\beta}_3$). (b) Energy densities in the shocked-plasma regions (2) and (3). (c) Energy per particle, e_i/n_i in the shocked-plasma regions (2) and (3). (d) Adiabatic indeices $\hat{\gamma}_i$ in the four different regimes.

and (3) as a function of $\Gamma_4\beta_4$. The analytic approximations in the relativistic regime (Equation (9)) and nonrelativistic regime (Equation (17)) again provide an excellent description of the thermodynamical properties of the plasma. The transition between the nonrelativistic and relativistic regimes occurs for those values of $\Gamma_4\beta_4$ in which $\Gamma_2\beta_2/\bar{\Gamma}_3\bar{\beta}_3$ becomes relativistic. Finally, in Figure 1(d) we show the adiabatic indices in the different regimes. While clearly $\hat{\gamma}_1 = \hat{\gamma}_4 = 5/3$, the adiabatic indices of the shocked plasma are gradually changing as $\Gamma_4\beta_4$ increases, and the shocked plasma is heated.

In Figure 2 we consider a more complicated scenario, that of a collision between two cool shells. We chose as parameters $n_1 = 99.99\ \mathrm{cm}^{-3}$, $\epsilon_1 = 0.01\ \mathrm{erg\ cm}^{-3}$ (namely, $e_1 = 100\ \mathrm{erg\ cm}^{-3}$), $n_4 = 4.99\ \mathrm{cm}^{-3}$ and $\epsilon_4 = 0.01\ \mathrm{erg\ cm}^{-3}$. Similar to the previous example, we took $\beta_1 = 0$, namely, a slow shell at rest. These values are chosen for presentation purposes, as we wish to ensure a good contrast of the shocked-plasma properties between the different regimes.

The velocities of the shocked-plasma regions (2) and (3) as measured in the rest-frames of the slow-plasma shell ($\Gamma_2\beta_2$) and the fast-plasma shell ($\bar{\Gamma}_3\bar{\beta}_3$) are shown in Figure 2(a). The analytical approximation in the relativistic regime (Equation (8)) and the nonrelativistic regime (Table 1(d)) provide excellent aproximations in the two regimes. The decay of the analytical approximation to $\bar{\beta}_3 = \beta_4 - \beta_2$ around $\Gamma_4 \sim 1$ arises from the use of $\Gamma_4\beta_4$ in the calculation of β_2.

The ratio of densities across the forward shock is shown in Figure 2(b), together with the analytic approximations. There are clearly three distinct regimes. First, there is the relativistic regime, $\Gamma_2 \gg 1$. In this regime, the density ratio is well

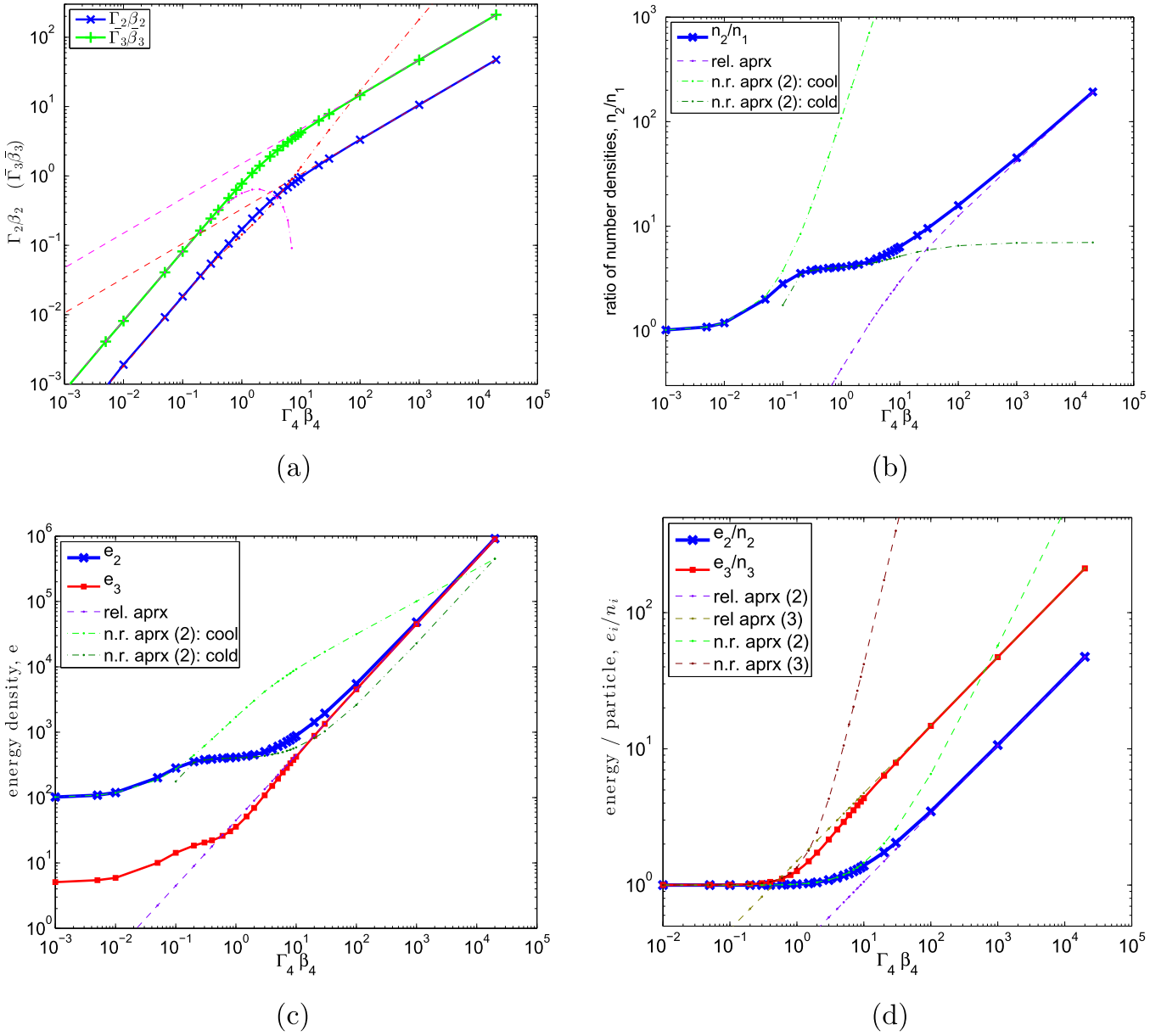

Figure 2. Velocities and thermodynamic properties of the shocked plasma following collision between two cool plasma shells ($\epsilon_i/n_i \ll 1$, $i = 1, 4$). The parameters considered are $n_1 = 99.99$ cm^{-3}, $\epsilon_1 = 0.01$ erg cm^{-3}, $n_4 = 4.99$ cm^{-3}, $\epsilon_4 = 0.01$ erg cm^{-3}, and $\beta_1 = 0$. Plasma parameters are shown as a function of the fast-shell initial velocity, $\Gamma_4\beta_4$. (a) Velocities of the shocked plasma (same as in Figure 1(a)) for a collision of cool plasma shells. (b) Ratio of number densities across the forward shock, n_2/n_1. (c) Energy densities in the shocked-plasma regions (2) and (3). (d) Energy per particle, e_i/n_i in the shocked-plasma regions (2) and (3).

approximated by the results given in Equation (7). A second regime is the nonrelativistic "cold" regime, namely $\beta_2 \geqslant \sqrt{2\epsilon_1/n_1} = 0.014$ (in the considered scenario), in which the density ratio is well approximated by Equation (17). Finally, when $\beta_2 \ll \sqrt{2\epsilon_1/n_1}$, the approximation in the "cool" regime given in Equation (16) provides a good fit to the density ratio. These same three regimes are also clearly observed when considering the energy densities of the shocked plasma in Figure 2(c). Interestingly, when considering the ratio e_i/n_i (Figure 2(d)) in the nonrelativistic regime, the cool and cold approximations can be combined to provide a good approximation, which reads $e_2/n_2 \simeq 1 + (\epsilon_1/n_1) + (\Gamma_2\beta_2)^2/2$. In the relativistic regime, this ratio is well described by Equation (9).

In Figure 3 we provide a third example, that of a collision between two initially hot plasma shells. As initial parameters, we chose $n_1 = 1$ cm^{-3}, $e_1 = 15$ erg cm^{-3}, $n_4 = 1$ cm^{-3}, $e_4 = 10$ erg cm^{-3}, and $\beta_1 = 0$.

For this choice of parameters, the results of Table 1(f) show a minimum value of β_4, below which two shock waves cannot form: for $\beta_4 = \sqrt{3}\,(\epsilon_1 - \epsilon_4)/4\epsilon_4 \simeq 0.24$, and $\beta_2 \to 0$. This is clearly demonstrated in Figure 3(a). At a higher relative velocity, the results in Equation (8) and Table 1 (f) provide an excellent approximation to the shocked-plasma velocity. The ratio of number densities across the forward shock, n_2/n_1 (Figure 3(b)) is well approximated by the analytical approximations in Equations (7) (relativistic) and 13 (nonrelativistic). Similarly, the energy per particle in the shocked regions (2) and (3) shown in Figure 3(c) are well approximated by the analytical result in Equation (9) in the relativistic regime and by $e_2/n_2 \simeq (e_1/n_1)(1 + \Gamma_2\beta_2/\sqrt{3} + (\Gamma_2\beta_2)^2/6)$ in the

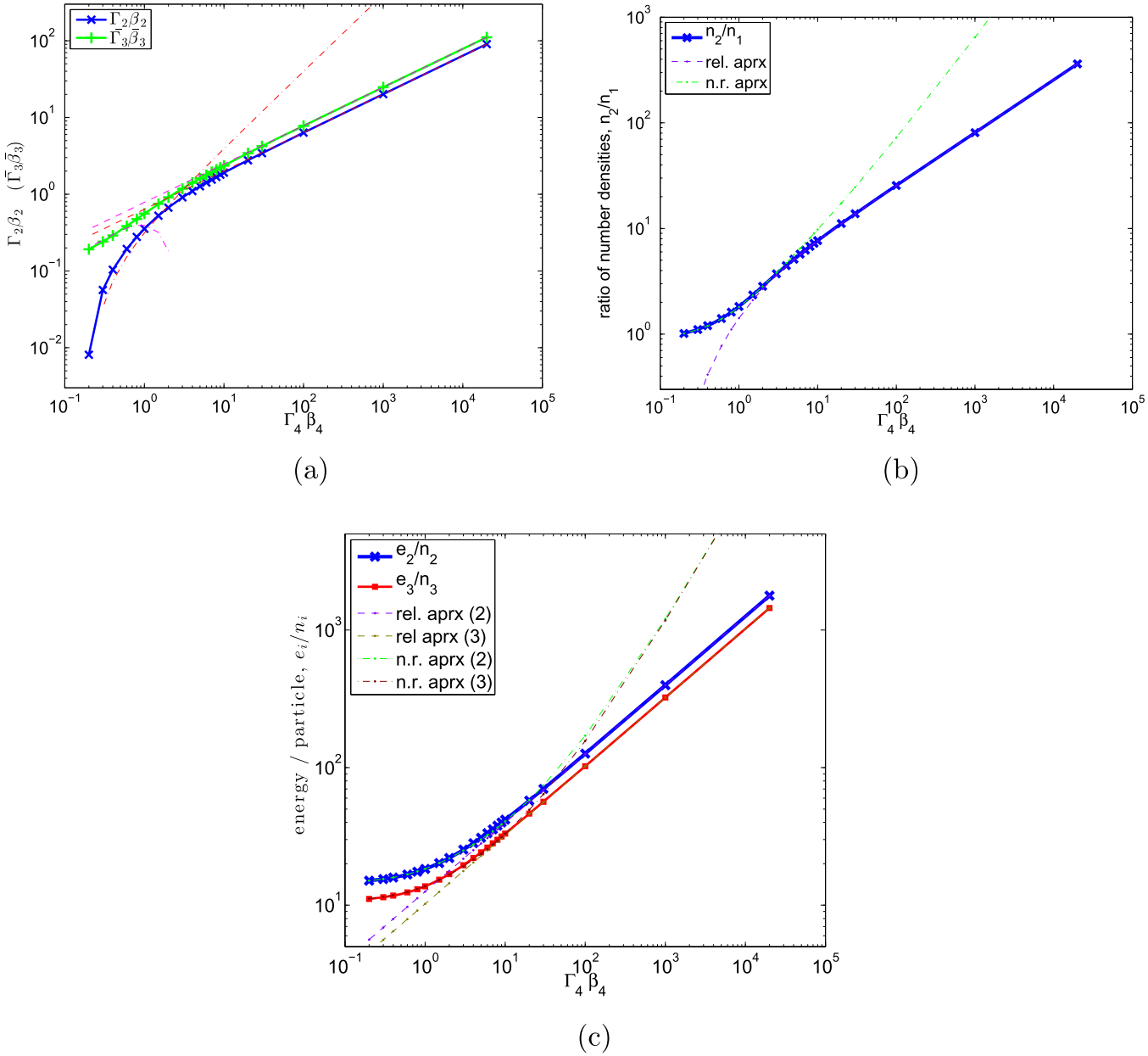

Figure 3. Velocities and thermodynamic properties of the shocked plasma following collision between two initially hot ($\epsilon_i/n_i \gg 1$) plasma shells. Parameters considered are $n_1 = 1$ cm^{-3}, $e_1 = 15$ erg cm^{-3}, $n_4 = 1$ cm^{-3}, $e_4 = 10$ erg cm^{-3}, and $\beta_1 = 0$. Plasma parameters are shown as a function of the fast-shell initial velocity, $\Gamma_4\beta_4$. (a) Velocities of the shocked plasma (same as in Figure 1(a)) for a collision of two hot plasma shells. (b) Ratio of number densities across the forward shock, n_2/n_1. (c) Energy per particle, e_i/n_i in the shocked-plasma regions (2) and (3).

nonrelativistic regime, which is readily derived from Equations (13) and (14).

4. Observational Consequences

4.1. Efficiency in Kinetic Energy Dissipation

The calculations above enable us to determine the efficiency of kinetic energy conversion during two shell collisions. Various authors have calculated this efficiency using an integral approach, namely by determining the merged-shell bulk Lorentz factor assuming a plastic collision between the two shells, and using conservations of energy and momentum. For example, Kobayashi et al. (1997) and Malzac (2014) considered cold-plasma shells, while Spada et al. (2001) and Jamil et al. (2010) generalized the result to hot plasmas.

Using the formulation developed here, we can generalize these results. The calculation is made in the rest-frame of the shocked plasma. In this frame, the slow shell in region (1) is seen to have a Lorentz factor $\tilde{\Gamma}_1$ (corresponding velocity $\tilde{\beta}_1$), where $\tilde{\Gamma}_1\tilde{\beta}_1 = \Gamma_1\Gamma_2(\beta_1 - \beta_2)$. The transfer of momentum from the slow shell (region (1)) to the shocked plasma (region (2)), assuming a planar symmetry along the x direction, is given by

$$dP^x(1) = \int dV_1' T^{01} = \int dV_1' \omega_1 \tilde{\Gamma}_1^2 \tilde{\beta}_1 = \int dV_1 \omega_1 \tilde{\Gamma}_1 \tilde{\beta}_1. \quad (23)$$

Here, $dV_1' = dV_1/\tilde{\Gamma}_1$ is the volume element of material in region (1) that crosses the forward shock into region (2) per unit time, as

seen in the rest-frame of shocked region (2), and dV_1 is the same volume element as measured in the rest-frame of region (1).

Using $\omega_1 = n_1 + \hat{\gamma}_1 \epsilon_1$, as well as $dM_1 = \int dV_1 n_1$ and $dE_{\rm th,1} = \int dV_1 \epsilon_1$, the momentum transfer rate can be written as

$$dP^x(1) = (dM_1 + \hat{\gamma}_1 dE_{\rm th,1})\tilde{\Gamma}_1\tilde{\beta}_1, \quad (24)$$

where we assumed that the velocities are not changed during the shock propagation.

A similar calculation holds for the momentum transfer from the fast plasma (region (4)), which could be written as

$$dP^x(4) = (dM_4 + \hat{\gamma}_4 dE_{\rm th,4})\bar{\Gamma}_3\bar{\beta}_3, \quad (25)$$

where $\bar{\Gamma}_3\bar{\beta}_3 = \Gamma_4\Gamma_2(\beta_4 - \beta_2)$. Equating the momentum transfer on both sides leads to the velocity at the center-of-mass frame, which is the shocked-fluid frame as long as both shocks exist,

$$\beta_2 = \frac{\Gamma_1\beta_1(dM_1 + \hat{\gamma}_1 dE_{\rm th,1}) + \Gamma_4\beta_4(dM_4 + \hat{\gamma}_4 dE_{\rm th,4})}{\Gamma_1(dM_1 + \hat{\gamma}_1 dE_{\rm th,1}) + \Gamma_4(dM_4 + \hat{\gamma}_4 dE_{\rm th,4})}. \quad (26)$$

In the ultrarelativistic case, $\Gamma_4 \gg \Gamma_2 \gg 1$ this can be written as

$$\Gamma_2 \simeq \left(\frac{\Gamma_1(dM_1 + \hat{\gamma}_1 dE_{\rm th,1}) + \Gamma_4(dM_4 + \hat{\gamma}_4 dE_{\rm th,4})}{(dM_1 + \hat{\gamma}_1 dE_{\rm th,1})/\Gamma_1 + (dM_4 + \hat{\gamma}_4 dE_{\rm th,4})/\Gamma_4}\right)^{1/2}. \quad (27)$$

This result differs from the result that appears in Spada et al. (2001) (their Equation (4)) as well as from the result in Jamil et al. (2010) by the inclusion of the adiabatic indices $\hat{\gamma}_i$ that multiply the thermal energies, which are omitted in these works. These can be traced back to the inclusion of the pressure term in the shocked plasma.

We further point out that equating the momenta transfer from regions (1) and (4) using Equations (24) and (25) in the relativistic case would retrieve Equation (8). These results imply that the efficiency of kinetic energy conversion as calculated in Spada et al. (2001) and Jamil et al. (2010) holds provided that the final Lorentz factor is calculated using Equation (27).

4.2. Basic Scalings of Synchrotron Emission

The heated shocked plasma will radiate its energy. The observed signal can therefore be used as a probe of the initial unshocked-plasma shell properties. Full radiative calculations require additional parameters, such as the exact value of the magnetic field, as well as assumptions about the radiating particle distribution in the shocked-plasma regions, and are therefore left for a future work.

Here, we provide some basic scaling laws of the characteristic frequencies expected from synchrotron emission, which is likely the easiest (and most commonly discussed) signal that can be detected, and can therefore be used to probe the plasma conditions. These are particularly simple in the relativistic regime, where the plasma is substantially heated by the shock waves. We therefore focus here on the relativistic regime.

We scale the properties of the synchrotron emission in region i by adopting the common assumption that magnetic fields are generated by the shock waves and that the generated magnetic energy density is some constant fraction of the post-shock thermal energy density, namely $B_i^2 \propto e_i$. Furthermore, we assume that the electrons carry some constant fraction of the proton energy, resulting in a typical electron Lorentz factor $\gamma_{{\rm el},i} \propto (e_i/n_i)$. As the characteristic synchrotron emission frequency is $\nu_{\rm syn,i} \propto B_i\gamma_{{\rm el},i}^2$, one finds the scaling

$$\frac{\nu_{\rm syn,2}}{\nu_{\rm syn,3}} \propto \frac{e_2^{1/2}\left(\frac{e_2}{n_2}\right)^2}{e_3^{1/2}\left(\frac{e_3}{n_3}\right)^2} = \left(\frac{n_4}{n_1}\right)^2\left(\frac{\omega_1}{\omega_4}\right). \quad (28)$$

If we denote by Δ_1 and Δ_4 the (comoving) widths of the colliding shells, the total number of radiating electrons is $N_1 \propto n_1\Delta_1$ and $N_4 \propto n_4\Delta_4$ (under the 1D assumption). Since the total observed power is $P_{\rm syn} \propto NB^2\gamma_{\rm el}^2$ (Rybicki & Lightman 1979), the ratio of synchrotron power between the two shocked regions is

$$\frac{P_{\rm syn,2}}{P_{\rm syn,3}} = \frac{n_1\Delta_1 e_2\left(\frac{e_2}{n_2}\right)^2}{n_4\Delta_4 e_3\left(\frac{e_3}{n_3}\right)^2} = \left(\frac{\Delta_1}{\Delta_4}\right)\left(\frac{n_4}{n_1}\right)\left(\frac{\omega_1}{\omega_4}\right). \quad (29)$$

In the relativistic scenario, the observed timescale for the forward-shock wave to cross the slow-plasma shell is $\sim\Delta_1\Gamma_1/c$, while the timescale of the reverse shock to cross the fast plasma is $\approx\Delta_4\Gamma_2^2/\Gamma_4 c \sim 2\Gamma_1(\omega_4/\omega_1)\Delta_4 c$ (e.g., Sari & Piran 1995). Thus, the observed ratio of the timescale of existence of the two shock waves is

$$\frac{t_{fs}}{t_{rs}} = \left(\frac{\Delta_1}{\Delta_4}\right)\left(\frac{\omega_1}{\omega_4}\right). \quad (30)$$

These results imply that identification of the ratios of the three main characteristics of synchrotron emission from the forward-shock and reverse-shock waves, namely the characteristic frequency, total power, and timescales, are sufficient to provide direct information about the ratio of number densities, enthalpies, and initial sizes of the colliding shells. Interestingly, in the ultrarelativistic limit, these results are independent of the unknown Lorentz factor. As we showed above, using these initial conditions, one can calculate the properties of the merged shell. Therefore, direct observations of multiple-shell collisions could provide information about two key ingredients. The first is the initial conditions of the ejected shells, hence the properties of the inner engine. The second is the temporal and hence spatial evolution (adiabatic losses) of the merged shell.

5. Summary and Discussion

In this work, we considered the collision of two plasma shells, as is expected in the "internal shock" model. We generalized previous treatments of the problem by considering plasmas that can be arbitrarily hot. This is a natural consequence of the internal-shocks scenario, as, after the first collision, the merged shell is inevitably hot (and can be very hot if the shells are relativistic, see Equation (9)). We point out that while in between collisions the colliding shells lose their energy adiabatically, the decrease in temperature (or energy per particle) is $(e/n) \propto T \propto r^{-2/3}$, and thus even if the internal collisions occur within a range of several orders of magnitude in radii, adiabatic cooling is not sufficient to completely cool the plasma shells.

We derived analytical approximations for the shocked-shell velocities in both the relativistic (Equation (8)) and nonrelativistic (Table 1) regimes. A very important result we found is that in the general scenario (as opposed to the cold scenario), there is a minimum relative velocity, or Lorentz factor, that enables the formation of the two-shock system (Equation (10)). The physical reason for this is the requirement of the ram pressure to exceed the pressure associated with the excess of thermal energy caused by the shock. If this criterion is not met, only a single-shock wave is expected, while a rarefaction wave will propagate into the hotter plasma. In this case, we expect the radiative signal to be much weaker.

We furthermore provided analytical expressions for the energy density and for the energy per particle in the shocked region. We found that for nonrelativistic collision, one needs to discriminate between three scenarios: "hot" plasma, for which $\epsilon/n \gg 1$, "cool" plasmas for which $1 \gg \epsilon/n \gg \beta^2$, and "cold" plasma, for which $1 \gg \beta^2 \gg \epsilon/n$. We provided the analytical expressions for thermodynamical properties of the shocked plasma in each of these cases.

We discussed several observational consequences of the dynamical results. We showed that in calculating the final Lorentz factor of the merged shell, hence the efficiency of kinetic energy dissipation, one needs to consider the pressure of the shocked plasma. We provided the basic scaling laws of synchrotron emission in the ultrarelativistic regime and showed that measurements of the peak energy, flux, and timescale of emission enables one to deduce important information about the initial shells properties, as well as the spatial evolution of the propagating shells.

The results provided here emphasize the fact that the properties of the shocked plasma depend not only on the relative velocities between the colliding plasma shells, but also on the energy per particle in each colliding shell. These results are therefore important in the study of signals from multiple collisions that are expected in various environments, such as GRBs, XRBs, and AGNs. Furthermore, our numerical results are particularly useful for probing the plasma properties in the transrelativistic regime, which is likely the dominant regime in XRBs and possibly in AGNs. As we demonstrated in Section 3 above, while no simple analytical expressions exist in this regime, reasonable analytical fits still do exist, and can be very useful in understanding the underlying properties of these objects.

The results obtained in this work imply that the overall efficiency of kinetic energy dissipation in a multiple-shock scenario is in general different than previous calculations that considered collisions between cold shells (Kobayashi et al. 1997; Daigne & Mochkovitch 1998; Lazzati et al. 1999; Beloborodov 2000; Kumar 2000; Guetta et al. 2001; Ioka et al. 2006). In a realistic scenario of hot shells, when estimating the efficiency in multiple-shell collisions, one needs to consider (i) the properties of each shell immediately after the collision; (ii) the adiabatic cooling of the shells in between the collisions; and (iii) the adiabatic expansion of each shell in between collisions, which results in a differential velocity field within the expanding shell (Kobayashi & Sari 2001). In this work we focused on part (i) of this problem. We leave a complete treatment of a multiple-shell collision scenario for a future work.

A.P. wishes to thank Damien Bégué Felix Ryde, Ralph Wijers, and Bing Zhang for useful comments. This research was partially supported by the European Union Seventh Framework Programme (FP7/2007-2013) under grant agreements n° 618499 (AP) and n° 322259 (PC).

ORCID iDs

Asaf Pe'er https://orcid.org/0000-0001-8667-0889

References

Axelsson, M., Baldini, L., Barbiellini, G., et al. 2012, ApJL, 757, L31
Beloborodov, A. M. 2000, ApJL, 539, L25
Blandford, R. D., & McKee, C. F. 1976, PhFl, 19, 1130
Böttcher, M., & Dermer, C. D. 2010, ApJ, 711, 445
Cantó, J., Lizano, S., Fernández-López, M., González, R. F., & Hernández-Gómez, A. 2013, MNRAS, 430, 2703
Coroniti, F. V. 1990, ApJ, 349, 538
Daigne, F., & Mochkovitch, R. 1998, MNRAS, 296, 275
Drappeau, S., Malzac, J., Belmont, R., Gandhi, P., & Corbel, S. 2015, MNRAS, 447, 3832
Drenkhahn, G. 2002, A&A, 387, 714
Drenkhahn, G., & Spruit, H. C. 2002, A&A, 391, 1141
Fender, R. P. 2001, MNRAS, 322, 31
Fenimore, E. E., Madras, C. D., & Nayakshin, S. 1996, ApJ, 473, 998
Fox, D. B., & Mészáros, P. 2006, NJPh, 8, 199
Freedman, D. L., & Waxman, E. 2001, ApJ, 547, 922
Gehrels, N., Ramirez-Ruiz, E., & Fox, D. B. 2009, ARA&A, 47, 567
Ghisellini, G. 1999, AN, 320, 232
Guetta, D., Spada, M., & Waxman, E. 2001, ApJ, 557, 399
Guiriec, S., Connaughton, V., Briggs, M. S., et al. 2011, ApJL, 727, L33
Ioka, K., Toma, K., Yamazaki, R., & Nakamura, T. 2006, A&A, 458, 7
Jamil, O., Fender, R. P., & Kaiser, C. R. 2010, MNRAS, 401, 394
Kaiser, C. R., Sunyaev, R., & Spruit, H. C. 2000, A&A, 356, 975
Kino, M., Mizuta, A., & Yamada, S. 2004, ApJ, 611, 1021
Kobayashi, S., Piran, T., & Sari, R. 1997, ApJ, 490, 92
Kobayashi, S., & Sari, R. 2001, ApJ, 551, 934
Kumar, P. 2000, ApJL, 538, L125
Kumar, P., & Piran, T. 2000, ApJ, 532, 286
Kumar, P., & Zhang, B. 2015, PhR, 561, 1
Lazzati, D., Ghisellini, G., & Celotti, A. 1999, MNRAS, 309, L13
Lazzati, D., Morsony, B. J., & Begelman, M. C. 2009, ApJL, 700, L47
Lyubarsky, Y., & Kirk, J. G. 2001, ApJ, 547, 437
Malzac, J. 2013, MNRAS, 429, L20
Malzac, J. 2014, MNRAS, 443, 299
Marscher, A. P. 1980, ApJ, 235, 386
Mészáros, P. 2006, RPPh, 69, 2259
Mészáros, P., Ramirez-Ruiz, E., Rees, M. J., & Zhang, B. 2002, ApJ, 578, 812
Meszaros, P., & Rees, M. J. 2014, arXiv:1401.3012
Miller-Jones, J. C. A., McCormick, D. G., Fender, R. P., et al. 2005, MNRAS, 363, 867
Mimica, P., & Aloy, M. A. 2010, MNRAS, 401, 525
Nakar, E., & Piran, T. 2002, ApJL, 572, L139
Norris, J. P., Nemiroff, R. J., Bonnell, J. T., et al. 1996, ApJ, 459, 393
Panaitescu, A., Spada, M., & Mészáros, P. 1999, ApJL, 522, L105
Pe'er, A. 2008, ApJ, 682, 463
Pe'er, A. 2014, SSRv, 183, 371
Pe'er, A. 2015, AdAst, 2015, 907321
Piran, T. 2004, RvMP, 76, 1143
Ramirez-Ruiz, E., & Fenimore, E. E. 2000, ApJ, 539, 712
Rees, M. J. 1978, MNRAS, 184, 61P
Rees, M. J., & Meszaros, P. 1994, ApJL, 430, L93
Rybicki, G. B., & Lightman, A. P. 1979, Radiative Processes in Astrophysics (New York: Wiley)
Ryde, F. 2004, ApJ, 614, 827
Ryde, F. 2005, ApJL, 625, L95
Ryde, F., & Pe'er, A. 2009, ApJ, 702, 1211
Ryde, F., Pe'er, A., Nymark, T., et al. 2011, MNRAS, 415, 3693
Sari, R., & Piran, T. 1995, ApJL, 455, L143
Sari, R., & Piran, T. 1997, ApJ, 485, 270

Service, A. T. 1986, ApJ, 307, 60
Sikora, M., Begelman, M. C., & Rees, M. J. 1994, ApJ, 421, 153
Spada, M., Ghisellini, G., Lazzati, D., & Celotti, A. 2001, MNRAS, 325 1559
Thompson, C. 1994, MNRAS, 270, 480
Usov, V. V. 1992, Natur, 357, 472
Wang, F. Y., & Cheng, K. S. 2012, MNRAS, 421, 908
Wiersma, J. 2007, PhD thesis, Utrecht Univ.
Woosley, S. E., & Bloom, J. S. 2006, ARA&A, 44, 507
Zhang, B. 2007, ChJAA, 7, 1
Zhang, B. 2014, IJMPD, 23, 30002
Zhang, B., & Mészáros, P. 2002, ApJ, 566, 712